Bounded inhomogeneous wave profiles for increased surface wave excitation efficiency at fluid–solid interfaces

Daniel C. Woods, J. Stuart Bolton, and Jeffrey F. Rhoads[a)]
School of Mechanical Engineering, Ray W. Herrick Laboratories, and Birck Nanotechnology Center, Purdue University, West Lafayette, Indiana 47907, USA

(Received 13 June 2016; revised 5 March 2017; accepted 20 March 2017; published online 20 April 2017)

Though the ultrasonic excitation of surface waves in solids is generally realized through the use of a contact transducer, remote excitation would enable standoff testing in applications such as the nondestructive evaluation of structures. With respect to the optimal incident wave profile, bounded inhomogeneous waves, which include an exponentially decaying term, have been shown to improve the surface wave excitation efficiency as compared to Gaussian and square waves. The purpose of this work is to investigate the effect of varying the incident wave spatial decay rate, as applied to both lossless fluid–solid interfaces and to solids with viscoelastic losses included. The Fourier method is used to decompose the incident profile and subsequently compute the reflected wave profile. It is shown that inhomogeneous plane wave theory predicts, to a close approximation, the location of the minimum in the local reflection coefficient with respect to the decay rate for bounded incident waves. Moreover, plane wave theory gives a reasonable indication of the decay rate that maximizes the surface wave excitation efficiency. © *2017 Acoustical Society of America*.
[http://dx.doi.org/10.1121/1.4979595]

[KML] Pages: 2779–2787

I. INTRODUCTION

The excitation of surface waves on solid media is of interest in a number of contexts, including nondestructive testing[1,2] and seismology.[3] Though in typical applications body and surface waves are excited in the solid by means of a contact transducer, remote, non-contact excitation would enable testing from a standoff distance, which may prove useful, for instance, in the nondestructive evaluation of structures,[4–6] in medical ultrasound imaging,[7,8] and in other applications where the use of a couplant is undesirable.[9–11] The excitation of Rayleigh-type surface waves by incident acoustic plane waves has previously been considered in depth,[12–14] as has the excitation by bounded incident waves having a Gaussian profile.[15–18] More recently, excitation by other types of bounded ultrasonic beams has been investigated experimentally and has been confirmed to produce both specular and nonspecular reflected portions, corresponding to subsurface transmission and the excitation of solid surface waves.[19–21] However, little attention has been given to the effect of tuning the waveform to enhance the surface wave excitation efficiency.

To this end, Vanaverbeke *et al.*[22] considered more general incident wave profiles, termed "bounded inhomogeneous waves," where a component of exponential decay was introduced perpendicular to the propagation direction. Their work drew a strong connection between the reflection and transmission of the bounded incident waves at the fluid–solid interface and inhomogeneous plane wave theory, where the local reflection coefficient in the specular direction was observed to remain close to that predicted by plane wave theory, particularly for larger beamwidths. More importantly, it was shown that the surface wave excitation efficiency for the bounded inhomogeneous incident waves was substantially higher than that for Gaussian and square profiles. Interestingly, previous work has shown that, by tuning the decay rate of incident inhomogeneous plane waves, a zero of the reflection coefficient can be achieved near the Rayleigh angle for lossless fluid–solid interfaces,[23] and near-zero values can be achieved for low-loss, viscoelastic fluid–solid interfaces.[24] Though Vanaverbeke *et al.*,[22] along with others,[13,21,25,26] have given a detailed account of the effects of the frequency, beamwidth, and steepness of the incident profiles, they have not reported tuning the decay parameter to improve the surface wave excitation efficiency.

It is thus the purpose of the present work to demonstrate that inhomogeneous plane wave theory can be used to approximate the optimal spatial decay rate of bounded incident waves that maximizes the surface wave excitation efficiency near the Rayleigh angle. Moreover, these predictions for lossless solid interfaces will be extended to low-loss viscoelastic solid interfaces by using the theory for linear viscoelastic media. In this effort, the form of the wave profile at the interface surface will be varied, in terms of the specified rate of spatial exponential decay and effective beamwidth, to investigate the effect on the surface wave generation.

With regard to the specification of the incident wave profile, in practice, the form may be prescribed at some standoff distance from the interface, in which case the propagation effect of the bounded wave over the nonzero offset distance would necessarily cause distortion of the profile at the interface surface. This effect on both the profile amplitude and phase, which may be of significant interest in a number of

[a)]Electronic mail: jfrhoads@purdue.edu

practical systems, is discussed in the Appendix. However, the aim of this work is to isolate the effect of the waveform parameters at the interface on the excitation efficiency, so the profile will be prescribed explicitly along the interface surface. Though considerations for a practical implementation of this condition lie beyond the scope of the present work, it should be noted here that, in a real system, this condition would need to be carefully controlled by appropriate sound field reproduction techniques,[27–29] in conjunction with fluid–coupled transducers, to ensure that the amplitude and phase information generated along the interface match (within an appropriate tolerance) that which is prescribed.

The well-known Fourier method[12,15–18,22] will be utilized in this work to compute the reflected wave profiles, from which the energy fluxes and surface wave excitation efficiency can be subsequently calculated. In addition to the excitation efficiency, the correspondence between the local reflection coefficient (taken at a specific point along the interface) as a function of the incident wave decay rate and that predicted by plane wave theory will also be presented.

II. FOURIER DECOMPOSITION OF BOUNDED INHOMOGENEOUS WAVE PROFILES

A bounded harmonic acoustic wave, with an arbitrary incident profile, in a semi-infinite fluid medium is considered here. The two-dimensional wave propagating in the xz-plane is incident on a solid interface, and the rectangular coordinate systems are shown in Fig. 1. The fluid is assumed to be linear, isotropic, homogeneous, and lossless. The solid is also assumed to be linear, isotropic, and homogeneous, but may be either lossless or linear viscoelastic.

By using the form presented by Vanaverbeke *et al.*[22] for the particle displacement, the wave potential of a longitudinal, bounded inhomogeneous incident wave can be modeled, in the frame of the wave and at $z' = 0$, by the analytical expression

$$\tilde{\phi}_{inc}(x',0) = \tilde{A} e^{\left[\beta x' - (1/p)(|x'|/W)^p\right]} e^{-j\omega t}, \tag{1}$$

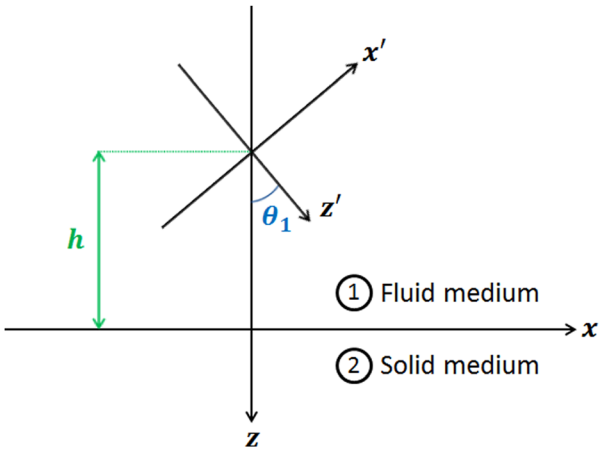

FIG. 1. (Color online) A diagram showing the rectangular coordinate systems at the fluid–solid interface. The unprimed system lies in the frame of the interface, and the primed system lies in the frame of the incident wave, which propagates in the positive z'-direction.

where β is the decay parameter, W is the half beamwidth, p is the steepness parameter, ω is the angular frequency, t is the time variable, and $\tilde{A}$ is the wave potential amplitude. This versatile form of the profile not only allows for an exponentially decaying term that is analogous to the decay of inhomogeneous plane waves perpendicular to the propagation direction,[23,30,31] but it also facilitates the modeling of other waveforms, including Gaussian and square profiles.[22] Note that the term "bounded" is used to describe profiles of this type since the amplitude takes on very small values outside of the spatial region near $x' = 0$, a spatial windowing which is controlled by the term $e^{-(1/p)(|x'|/W)^p}$ in Eq. (1). The function is, however, defined over the entire x'-axis.

The Fourier transform can be applied to this incident profile in a straightforward way in order to subsequently obtain the reflected wave profile in the frame of the interface (i.e., in the xz-frame). For the sake of brevity, the details of the derivation, which are given in the literature,[12,15–18,22,32] are omitted here. Since the goal of this work is to isolate the effect of the incident wave profile along the interface on the transmission characteristics, a parameterized form of the profile along x at $z = 0$ is employed here, using the limit as the offset distance h goes to zero. As was previously discussed, if nonzero distances h are considered, then the bounded profile along the interface is distorted relative to the incident profile. This propagation effect for bounded waves, along with appropriate equations and exemplary results, is discussed in the Appendix.

The parameterized form of the profile along the interface utilized here is the expression used by Vanaverbeke *et al.*,[22] where the profile in Eq. (1) is simply projected onto the interface surface,

$$\tilde{\phi}_{inc}(x,0) = \tilde{A} e^{\left[\beta_0 x - (1/p)(|x|/W_0)^p\right]} e^{j(k_0 x - \omega t)}, \tag{2}$$

where k_1 is the longitudinal material wave number in the fluid, $k_0 = k_1 \sin(\theta_1)$ is the x-component of the mean wave vector, $\beta_0 = \beta \cos(\theta_1)$ is the projected decay parameter, and $W_0 = W/\cos(\theta_1)$ is the projected half beamwidth. The term $e^{jk_0 x}$ gives the phase propagation of the incident wave along the interface, and the term $e^{\beta_0 x}$ is the spatial decay rate along the interface, which is directly analogous to the decay rate if the incident wave were an inhomogeneous plane wave. The Fourier transform in the interface frame is then given as

$$\tilde{F}_{inc}(k_x) = \int_{-\infty}^{+\infty} \tilde{\phi}_{inc}(x,0) e^{-jk_x x} \mathrm{d}x, \tag{3}$$

and the wave potential profile of the reflected wave is thus

$$\tilde{\phi}_R(x,0) = \frac{1}{2\pi} \int_{-\infty}^{+\infty} \tilde{R}(k_x) \tilde{F}_{inc}(k_x) e^{jk_x x} \mathrm{d}k_x, \tag{4}$$

where $\tilde{R}$ is the plane wave reflection coefficient, as defined in the literature for both the lossless fluid–solid interface[12] and the viscoelastic fluid–solid interface.[33–36]

III. EFFICIENCY OF RAYLEIGH-TYPE SURFACE WAVE EXCITATION

When a bounded acoustic beam is incident on a solid surface near the Rayleigh angle, a portion of the incident energy is transmitted into the solid and carried within the solid medium along the interface (i.e., in the x-direction in Fig. 1).[15,22,32] This energy flux generates a Rayleigh-type surface wave in the solid, which then reradiates energy into the fluid to form the displaced portion of the reflected profile. This shift of the reflected wave along the interface has been described in detail for Gaussian incident profiles[15,32] and for bounded inhomogeneous incident profiles.[13,20,22] There thus exists, near the incident beam, a power flux at any given position x along the interface which will be reradiated into the fluid by the excitation of the surface wave.

In order to quantify the surface wave generation by bounded inhomogeneous incident waves, the surface wave excitation efficiency, as a function of the position along the interface, can be defined as the difference between the incident and reflected intensities normal to the interface, integrated from $-\infty$ to x and normalized with respect to the total incident normal intensity[22,32]

$$\eta(x) = \frac{\int_{-\infty}^{x} \left[\, |I_{inc,z}(\xi,0)| - |I_{R,z}(\xi,0)| \,\right] \mathrm{d}\xi}{\int_{-\infty}^{+\infty} |I_{inc,z}(\xi,0)| \mathrm{d}\xi}, \tag{5}$$

where $I_{inc,z}$ and $I_{R,z}$ are the normal intensities of the incident and reflected waves, respectively. The intensities for each wave, denoted with the subscript m, are straightforward to compute in the lossless fluid as $I_{m,z} = \mathrm{Re}[-\tilde{\sigma}_{m,zz}\tilde{v}^{*}_{m,z}]/2$, where Re denotes the real part of the argument, $*$ denotes the complex conjugate, $\tilde{\sigma}_{m,zz} = -\rho_1\omega^2\tilde{\phi}_m$ is the associated normal stress (ρ_1 is the density of the fluid), and $\tilde{v}_{m,z}$ is the associated normal velocity

$$\begin{aligned} \tilde{v}_{inc,z}(x,0) &= \frac{\omega}{2\pi}\int_{-\infty}^{+\infty} \tilde{k}_z \tilde{F}_{inc}(k_x) e^{jk_x x} \mathrm{d}k_x, \\ \tilde{v}_{R,z}(x,0) &= \frac{\omega}{2\pi}\int_{-\infty}^{+\infty} -\tilde{k}_z \tilde{R}(k_x) \tilde{F}_{inc}(k_x) e^{jk_x x} \mathrm{d}k_x, \end{aligned} \tag{6}$$

where $\tilde{k}_z = \sqrt{k_1^2 - k_x^2}$ is evaluated as the principal square root[36] and is the z-component of the constituent wave vector. The surface wave excitation efficiency takes on its maximum value at a position $x_{\max}$, beyond which point the reflected normal intensity exceeds the incident intensity. However, it should be noted that, for the case of a plane incident wave, the excitation efficiency is independent of the position along the interface, since the ratio of the incident and reflected wave amplitudes is a function only of the plane wave reflection coefficient. Equation (5) thus simplifies, for a plane wave, to $\eta = 1 - |\tilde{R}|^2$.

It should be further emphasized here that the surface wave excitation efficiency in Eq. (5) and the incident and reflected profiles in Eqs. (2) and (4) specify the energy flux and pressure field at the interface (i.e., at any x-value along $z = 0$). Since this work is focused on finding the incident wave parameters which yield minimal reflection and maximal excitation efficiency at the interface, these quantities at $z = 0$ are sufficient. Note, however, that away from the interface, the reflected profile lies along a plane perpendicular to its associated mean wave vector, which is in general not aligned with the interface for oblique incidence.[13,19,22]

IV. NUMERICAL RESULTS AND DISCUSSION

In order to illustrate the effect of the spatial decay rate of the incident wave on the surface wave generation at fluid–solid interfaces, a water–stainless steel interface is considered here. The frequency was set to $f = 4$ MHz ($f = \omega/[2\pi]$), which is within the range for typical ultrasonic nondestructive testing applications. The densities and wave speeds of the two media were taken to be those used by Vanaverbeke *et al.*:[22] for water, density $\rho_1 = 1000\,\mathrm{kg/m^3}$ and longitudinal wave speed $c_1 = 1480$ m/s; and for stainless steel, density $\rho_2 = 7900\ \mathrm{kg/m^3}$, longitudinal wave speed $c_2 = 5790$ m/s, and shear wave speed $b_2 = 3100$ m/s. For the case in which viscoelastic losses in the stainless steel are included, which is considered in Sec. IV B, the longitudinal and shear wave attenuation coefficients at the given frequency were taken, respectively, to be $\alpha_{c_2} = 16.0$ rad/m and $\alpha_{b_2} = 50.8$ rad/m, which were computed from the inverse quality factors used by Borcherdt[36] for stainless steel. The steepness parameter in Eq. (1) was set to $p = 8$ for the bounded inhomogeneous incident profiles,[22] and the wave potential amplitude $\tilde{A}$ was taken to be an arbitrary constant.

To illustrate the form of the incident and reflected wave profiles, several incident profiles are presented in Fig. 2(a), and an incident profile along with the corresponding reflected profile at the lossless water–stainless steel interface are shown in Fig. 2(b), with incidence at $\theta_1 = 30.968°$, near the Rayleigh angle. The shift of the peak in the reflected wave profile along the interface is analogous to the shift observed for Gaussian incident waves.[15,32] For a detailed account of the form of the incident and reflected profiles, the reader is referred to the work of Vanaverbeke *et al.*[22]

In addition to the surface wave excitation efficiency defined by Eq. (5), the local reflection coefficient,[22] defined as the ratio $|\tilde{\phi}_R|/|\tilde{\phi}_{inc}|$, was considered at $x = z = 0$ as a measure of the local transmission efficiency at this point. Specifically, the effect of the decay parameter β was of interest here.

A. Water–stainless steel interface

For the lossless water–stainless steel interface, the magnitude of the reflection coefficient for an incident inhomogeneous plane wave and the magnitude of the local reflection coefficient for several bounded inhomogeneous incident waves are presented in Fig. 3 as a function of the decay parameter β. The waves are incident at the angle that minimizes the reflection coefficient, $\theta_1 = 30.968°$, which is near the Rayleigh angle. For the plane wave, the decay parameter gives the rate of exponential decay perpendicular to the propagation direction.[23,30,31] As is evident, the form of the plane wave reflection coefficient, including the location of the minimum, is closely matched by the local reflection

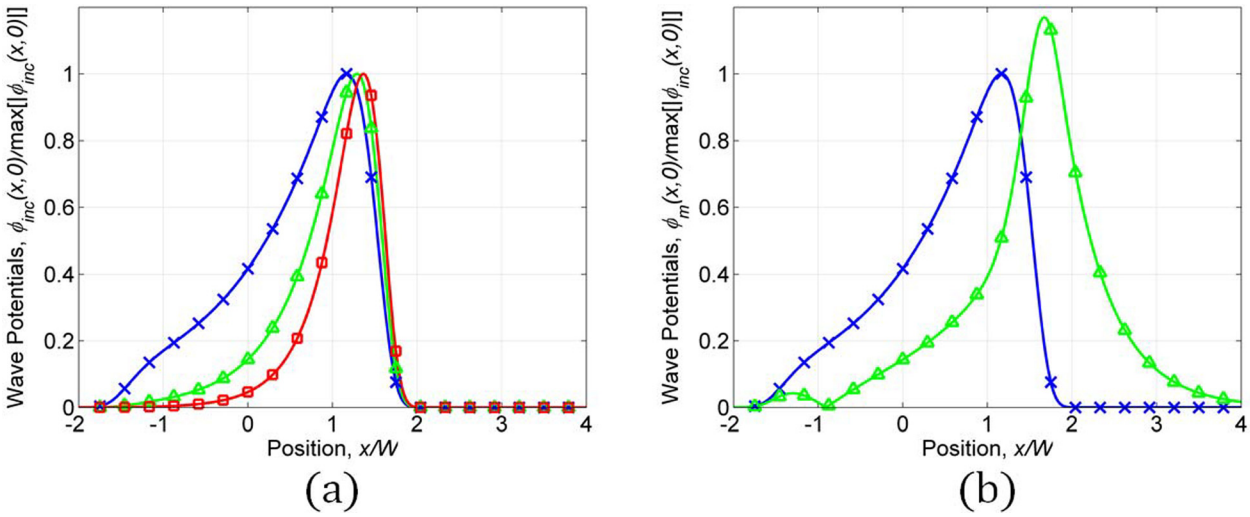

FIG. 2. (Color online) (a) Several incident bounded wave profiles ($p = 8$) of half beamwidth $W = 20$ mm, with decay parameters $\beta = 50$ rad/m ($\times$ markers), $\beta = 100$ rad/m (triangular markers), and $\beta = 200$ rad/m (square markers); and (b) an incident bounded wave profile ($W = 20$ mm, $\beta = 50$ rad/m, $p = 8$; $\times$ markers) along with the reflected wave profile (triangular markers) for the water–stainless steel interface at 4 MHz, with losses neglected.

coefficients for the wider beamwidths. The decay parameter which yields the minimum for the profile with the half beamwidth $W = 30$ mm is $\beta = 110.8$ rad/m, which gives a 0.18% error with respect to the value for the plane incident wave, $\beta = 111.0$ rad/m. Moreover, as expected, the correspondence between this decay value for bounded waves and that predicted by plane wave theory is found to be exact in the limit of large beamwidths. The profile with the smallest beamwidth in Fig. 3, however, shows a considerable shift to a lower value of the decay parameter required to yield the minimum. This is due to the fact that narrower beamwidths inherently possess a greater degree of inhomogeneity (as the spatial windowing dominates over a larger portion of the profile), and so less inhomogeneity must be introduced through the exponentially decaying term in order to achieve the optimal level of inhomogeneity. Also of note in Fig. 3(b) is the small nonzero value of the reflection coefficient at the minimum for the bounded wave profiles, as opposed to the zero value for the incident plane wave. The nonzero minimum value is attributable to the effect of the presence of the suboptimal wave vector components which are inherent in the bounded wave profile and which are quantified by the decomposition in Eq. (3).

Figure 4 shows the surface wave excitation efficiency, evaluated at the critical point $x_{\max}$ that yields the maximum efficiency, as a function of the decay parameter and half beamwidth of the incident wave. The global maximum of the excitation efficiency is observed at a decay parameter of $\beta = 134.2$ rad/m and a half beamwidth of $W = 7.7$ mm, which yield an efficiency of $\eta(x_{\max}) = 92.8\%$. Vanaverbeke *et al.*[22] noted the local maximum with respect to the beamwidth, and the results presented here indicate that a maximum with

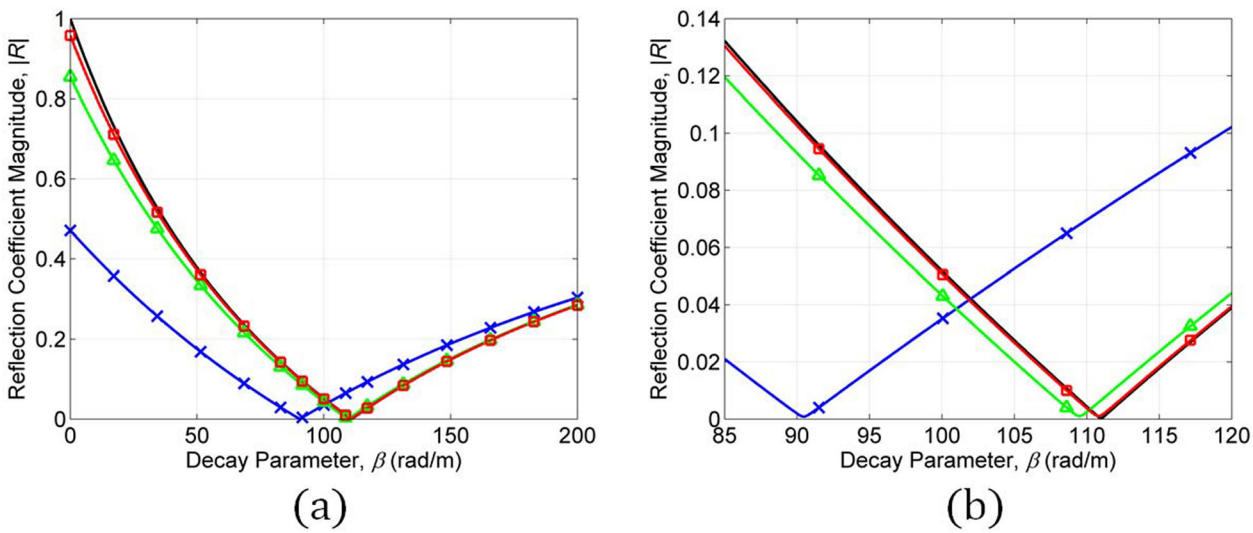

FIG. 3. (Color online) The magnitude of the reflection coefficient for the water–stainless steel interface at 4 MHz, with losses neglected, as a function of the incident wave decay parameter β. The incident waves are specified as an inhomogeneous plane wave (unmarked curve), and bounded wave profiles ($p = 8$) of half beamwidths $W = 10$ mm ($\times$ markers), $W = 20$ mm (triangular markers), and $W = 30$ mm (square markers). The curves for the inhomogeneous plane wave and bounded wave profile of half beamwidth $W = 30$ mm are nearly coincident. Note that (b) gives a zoomed-in view near the local minima.

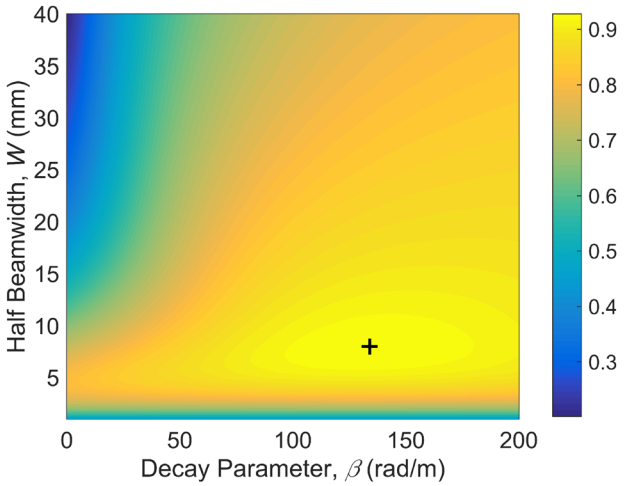

FIG. 4. (Color online) The surface wave excitation efficiency, evaluated at the critical point x_{max}, for the water–stainless steel interface at 4 MHz, with losses neglected, as a function of the incident wave decay parameter β and half beamwidth W for the bounded incident wave profiles ($p = 8$). The + marker indicates the global maximum.

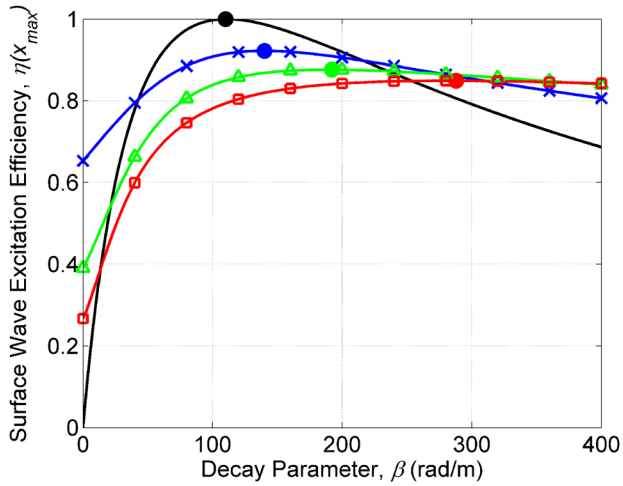

FIG. 5. (Color online) The surface wave excitation efficiency, evaluated at the critical point x_{max}, for the water–stainless steel interface at 4 MHz, with losses neglected, as a function of the incident wave decay parameter β. The incident waves are specified as an inhomogeneous plane wave (unmarked curve), and bounded wave profiles ($p = 8$) of half beamwidths $W = 10$ mm ($\times$ markers), $W = 20$ mm (triangular markers), and $W = 30$ mm (square markers). The solid, circular markers indicate the maxima for the respective incident waves.

respect to the decay parameter can also be located. As a point of comparison with more common incident wave profiles, the peaks in the excitation efficiency with respect to the beamwidth for Gaussian ($\beta = 0$, $p = 2$) and square ($\beta = 0$, $p = 8$) waves are found to be 80.2% and 80.9%, respectively. The use of the bounded inhomogeneous profiles considered here, with the optimal decay parameter and beamwidth, thus yields an improvement of approximately 12%–13% over those more common profiles. This improvement is even more pronounced for beamwidths which are larger than that at the peak value, and the relative increase in the excitation efficiency at a half beamwidth of 50 mm, for example, exceeds 50% as compared to both Gaussian and square incident waves (see also Ref. 22). As is evident in Fig. 4, the value of the decay parameter which yields the global maximum lies above the value which yields the reflection coefficient minimum, and this result is attributable to the greater spatial concentration of the incident wave's energy for the higher spatial decay rates. As such, the peak in the fraction of the power flux available for surface wave generation is larger for greater decay rates, and the energy is reradiated over a larger distance (i.e., the peak in the reflected wave profile is shifted farther along the interface). Moreover, for beamwidths larger than the width which yields the global maximum, the optimal decay parameter is shifted to higher values since the greater spatial concentration of the incident wave provided by larger decay values is more significant for the larger beamwidths. This effect is balanced by the increased transmission at the local minimum of the reflection coefficient at lower decay parameter values.

Figure 5 presents the surface wave excitation efficiency as a function of the decay parameter at the same half beamwidths as were used for calculating the reflection coefficients shown in Fig. 3, along with that for a plane incident wave, where the decay parameter range is increased to show the maximum for each beamwidth. For the plane wave, the peak in the excitation efficiency (which reaches an efficiency of 100%) is observed to occur at the exact decay value which yields the zero of the reflection coefficient, and the shift in the optimal decay rate to higher values for the bounded waves, which increases with beamwidth, is readily apparent. It should also be noted that, for the case of a homogeneous plane incident wave (i.e., $\beta = 0$), though stress fields are induced near the solid surface, at any given point along the interface, the energy from the incident wave is entirely reflected back into the fluid, and thus no energy is available for surface wave excitation at other points on the interface, which is shown by the zero value of the efficiency in Fig. 5.

B. Effect of viscoelastic losses in the solid medium

The effect of viscoelastic losses in the solid medium is considered here for the water–stainless steel interface. The magnitude of the reflection coefficient for an incident inhomogeneous plane wave and for several bounded inhomogeneous incident waves (using the local reflection coefficient) is presented in Fig. 6, with the waves again incident near the Rayleigh angle to minimize the reflection coefficient. It should be noted that this optimal angle, $\theta_1 = 30.973^\circ$, is slightly shifted relative to the lossless case. As is evident in Fig. 6, the main effect of the incorporation of the viscoelastic losses is the shift in the minimum of the reflection coefficient to significantly smaller values of the decay parameter. Since losses in the solid medium introduce additional levels of inhomogeneity in the transmitted waves, a smaller degree of inhomogeneity is necessary to optimize the transmission, as was previously noted for the case of incident inhomogeneous plane waves.[24] Moreover, the plane wave reflection coefficient magnitude remains less than unity even when the incident wave is homogeneous ($\beta = 0$), due to the losses in the solid. As can be observed, the reflection coefficients for the bounded wave profiles again closely match that of the plane wave for the larger beamwidths. Also of note is the increase

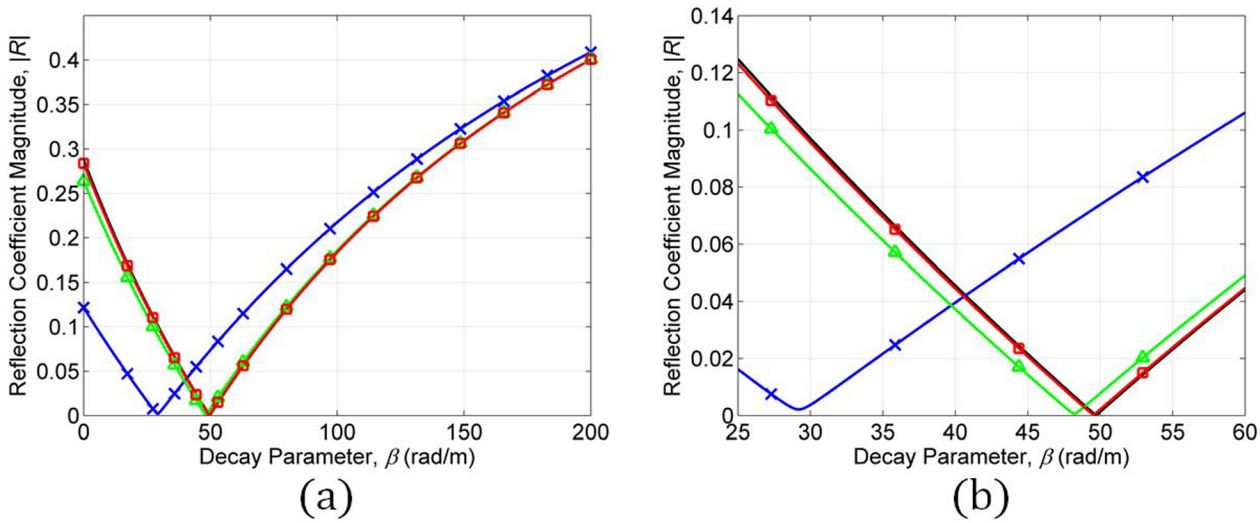

FIG. 6. (Color online) The magnitude of the reflection coefficient for the water–stainless steel interface at 4 MHz, with the viscoelastic losses in steel included, as a function of the incident wave decay parameter β. The incident waves are specified as an inhomogeneous plane wave (unmarked curve), and bounded wave profiles ($p = 8$) of half beamwidths $W = 10$ mm ($\times$ markers), $W = 20$ mm (triangular markers), and $W = 30$ mm (square markers). The curves for the inhomogeneous plane wave and bounded wave profile of half beamwidth $W = 30$ mm are nearly coincident. Note that (b) gives a zoomed-in view near the local minima.

in the reflection coefficient value at the minimum as compared to the lossless case, which is particularly evident for the narrowest beamwidth, $W = 10$ mm, in Fig. 6(b). This result also follows from the introduction of material damping, which increases the value at the local minimum.

Figure 7 shows the surface wave excitation efficiency, again evaluated at the critical point $x_{\max}$, as a function of the decay parameter and half beamwidth with the viscoelastic losses in stainless steel included. A global maximum can again be found but, with respect to the lossless case, the corresponding decay parameter is shifted to a lower value and the corresponding beamwidth is shifted to a higher value. This optimal decay rate, however, is still above the decay rate which yields the minimum of the reflection coefficient for the viscoelastic case. Interestingly, for beamwidths larger than that which yields the global maximum of the excitation efficiency, the optimal decay parameter decreases with increasing beamwidth, and this decay value ultimately falls below that which gives the reflection coefficient minimum. This effect may be due to the greater levels of inhomogeneity introduced in the transmitted waves by the material damping for the larger beamwidths, since these wave profiles experience the effects of the viscoelastic losses over a greater distance along the interface.

Finally, Fig. 8 gives the surface wave excitation efficiency as a function of just the decay parameter for the same half beamwidths as were previously considered, along with that for a plane incident wave. As for the lossless case, the

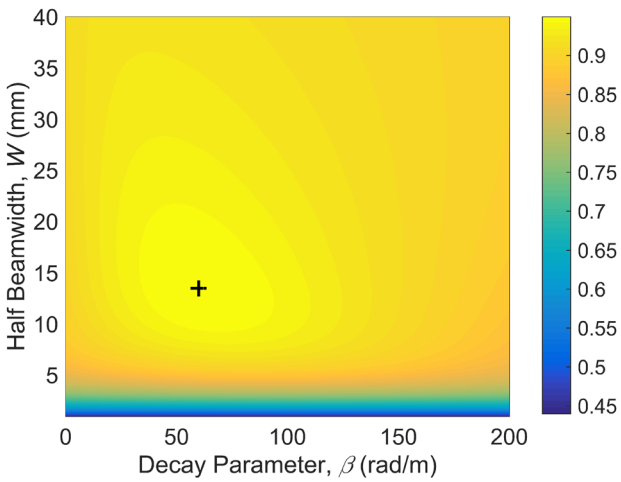

FIG. 7. (Color online) The surface wave excitation efficiency, evaluated at the critical point $x_{\max}$, for the water–stainless steel interface at 4 MHz, with the viscoelastic losses in steel included, as a function of the incident wave decay parameter β and half beamwidth W for the bounded incident wave profiles ($p = 8$). The + marker indicates the global maximum.

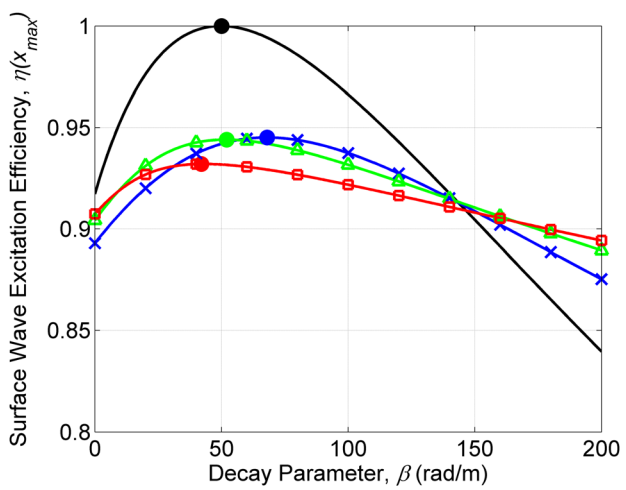

FIG. 8. (Color online) The surface wave excitation efficiency, evaluated at the critical point $x_{\max}$, for the water–stainless steel interface at 4 MHz, with the viscoelastic losses in steel included, as a function of the incident wave decay parameter β. The incident waves are specified as an inhomogeneous plane wave (unmarked curve), and bounded wave profiles ($p = 8$) of half beamwidths $W = 10$ mm ($\times$ markers), $W = 20$ mm (triangular markers), and $W = 30$ mm (square markers). The solid, circular markers indicate the maxima for the respective incident waves.

excitation efficiency for the plane incident wave reaches its maximum at the value of the decay parameter which yields the minimum of the reflection coefficient. Since the half beamwidth $W = 10\,\text{mm}$ lies below that which gives the global maximum for this case, the decay parameter which yields the peak efficiency is shifted to larger values, whereas the other two beamwidths shown in Fig. 8 lie above the global maximum and therefore show shifts to smaller decay parameter values to yield the respective peaks in excitation efficiency. Also note that the value of the efficiency for the homogeneous plane wave case ($\beta = 0$) is nonzero due to the losses in the solid. It follows that the excitation efficiency for the bounded wave profiles increases with increasing beamwidth in the limit of small values of the decay parameter.

V. CONCLUSIONS

A comparison of the predictions for the reflection coefficient and for the surface wave excitation efficiency of incident plane waves and incident bounded inhomogeneous waves as a function of the incident wave spatial decay rate has been presented for a lossless fluid–solid interface and also with viscoelastic losses included in the solid. This work extends that of Vanaverbeke *et al.*,[22] who demonstrated that bounded inhomogeneous waves improve the surface wave excitation efficiency as compared to Gaussian and square waves, by examining the effect of tuning the decay parameter. It was shown here that the minimum in the plane wave reflection coefficient with respect to the decay parameter[23,24] provides a good prediction of the minimum in the local reflection coefficient for bounded wave profiles, which is exact in the limit of large beamwidths. Inhomogeneous plane wave theory also provides an indication of the decay parameter value which maximizes the surface wave excitation efficiency, but this value is sensitive to the beamwidth of bounded waves and there is generally a shift to larger decay parameter values due to the greater spatial concentration of the incident wave energy at those larger decay rates. The incorporation of viscoelastic losses in the solid, however, has the effect of introducing additional inhomogeneity to the transmitted waves, and so lower values of the decay parameter were found to yield the maximum excitation efficiency with the losses included.

The results presented here, which demonstrate that an optimal value of the incident wave decay rate can be identified with incidence near the Rayleigh angle, may prove useful for non-contact excitation in applications such as nondestructive testing[1,2,4–6] and medical ultrasound imaging.[7,8] Moreover, these waveforms may be generated in practice by sound field reproduction techniques with phased arrays of sources,[29,37–39] or by other approaches,[27,28,31,40] though the distortion of the profile over nonzero standoff distances would have to be carefully controlled in such an implementation (see also the Appendix). The generation of bounded inhomogeneous waves of the type considered in this work, in particular, was investigated by Declercq and Leroy,[26] and it was noted that a reasonable approximation may be achievable in the near field.

In future work, sound field reproduction techniques for these types of bounded inhomogeneous wave profiles will be investigated, specifically through the use of source arrays. In addition, experimental validation of the theoretical predictions of the optimal surface wave excitation efficiency will be pursued. This work will continue the investigation of methods for increased acoustic transmission across fluid–solid interfaces through analysis and experimentation.

ACKNOWLEDGMENTS

This research is funded by the U.S. Office of Naval Research through ONR Grant Nos. N00014-10-1-0958 and N00014-16-1-2275.

APPENDIX: PROPAGATION EFFECT FOR BOUNDED INHOMOGENEOUS WAVES

With reference to Fig. 1, if the incident wave profile given by Eq. (1) is prescribed in the frame of the wave at $z' = 0$, then the Fourier decomposition into the plane wave spectrum must also be implemented at $z' = 0$. The associated Fourier transform is then[15,32]

$$\tilde{F}_{inc}(k_{x'}) = \int_{-\infty}^{+\infty} \tilde{\phi}_{inc}(x', 0) e^{-jk_{x'}x'} \mathrm{d}x'. \tag{A1}$$

The coordinate transformation to the interface frame is given by

$$\begin{aligned} x' &= x\cos(\theta_1) - (h+z)\sin(\theta_1), \\ z' &= x\sin(\theta_1) + (h+z)\cos(\theta_1). \end{aligned} \tag{A2}$$

Therefore, by using the coordinates and wave vector components in the interface frame, the incident wave profile can be written at an arbitrary position (where $z < 0$) as

$$\tilde{\phi}_{inc}(x, z) = \frac{1}{2\pi} \int_{-\infty}^{+\infty} \tilde{F}_{inc}(k_x) e^{jk_x x + jk_z(z+h)} \mathrm{d}k_x. \tag{A3}$$

To compute the reflected profile is also straightforward

$$\tilde{\phi}_R(x, z) = \frac{1}{2\pi} \int_{-\infty}^{+\infty} \tilde{R}(k_x) \tilde{F}_{inc}(k_x) e^{jk_x x - jk_z(z-h)} \mathrm{d}k_x. \tag{A4}$$

This approach to the computation of the profile at the interface (i.e., evaluating the expressions at $z = 0$) fully accounts for the propagation effect and resulting distortion of the bounded profile at the interface for arbitrary offset distances h. In the present work, the profile was instead prescribed along the interface itself, in order to isolate the effect of the wave profile alone. However, for the purpose of providing a brief discussion of this propagation effect, which is of interest in practical implementations, results for the distortion effect for several exemplary cases are presented here.

The water–stainless steel interface at 4 MHz considered in Sec. IV A is again considered here, with the incidence angle set at $\theta_1 = 30.968°$, near the Rayleigh angle. Figure 9 shows the amplitude distortion at the interface ($z = 0$) for an exemplary bounded wave profile of half beamwidth $W = 20\,\text{mm}$

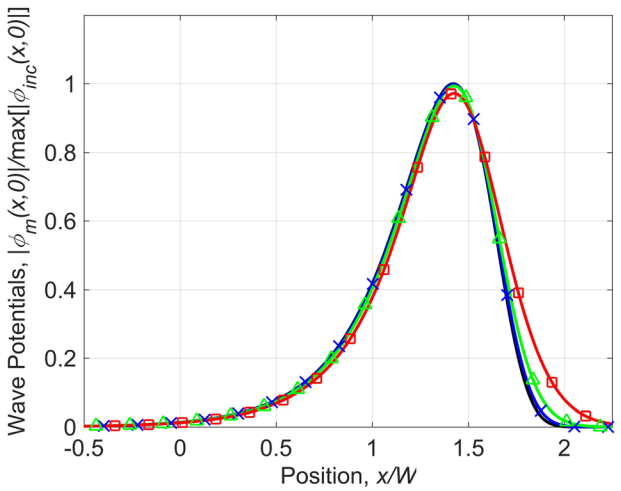

FIG. 9. (Color online) The amplitude distortion of an incident bounded wave profile at the interface ($z=0$) due to the propagation effect with the offset distance set at $h=0$ (unmarked curve), $h=25$ mm ($\times$ markers), $h=50$ mm (triangular markers), and $h=100$ mm (square markers). The incident wave has a half beamwidth of $W=20$ mm and a decay parameter of $\beta=200$ rad/m.

and decay parameter $\beta=200$ rad/m, given several values of the offset distance and corrected for the position of the peak. As is evident, the deviations relative to the undistorted profile ($h=0$) increase as the offset distance increases. Specifically, the profile for a distance of $h=25$ mm is nearly identical to the zero offset curve, but notable deviations on the right side of the profile are clear as the distance is increased to $h=50$ mm and $h=100$ mm.

In terms of the distortion of the phase, Fig. 10 presents the corresponding phase difference (in relation to the undistorted wave, $h=0$) for the same incident wave profiles. It should be clear that the offset distances constitute several wavelengths (approximately 68 wavelengths for $h=25$ mm, and a greater number for each of the larger offsets), so the phase difference in each case is shown relative to the value at an initial point for the reconstruction along the interface (i.e., a zero phase difference is taken at a point sufficiently to the left of the amplitude peak position). Since only the relative variations in the phase are significant (as the waves are harmonic), this constant offset does not impact the interpretation and facilitates a visualization of the phase distortion for all three cases. As is evident in Fig. 10, there is little variation up until the region approaching the amplitude peak near $x/W \approx 1.4$, where the phase lags behind that of the zero offset case, a lag which increases with offset distance. Beyond the location of the amplitude peak, the phase difference continues to decrease before climbing above the initial phase difference value due to the progressive decrease of the amplitude beyond the peak region. In this regime, though the phase continues to change relative to the zero offset profile, the corresponding amplitudes monotonically decrease to near-zero values. Thus, the phase difference has little effect on the reconstruction in this region. Note that the profile with an offset distance of $h=100$ mm shows the slowest phase variation beyond the amplitude peak, as this profile with the largest offset distance also shows the slowest convergence of the amplitude to zero in Fig. 9.

In light of the exemplary results shown here, the specification of the profile in the frame of the wave at some distance from the interface can be observed to introduce additional variability into the profile impinging at the interface, which is dependent not only on the distance h, but also on the form of the profile, the incidence angle, and the frequency. It therefore follows that the interface phenomena for bounded incident waves, such as the surface wave excitation, are dependent on that offset distance and those other parameters. This observation suggests that future work in the design of practical systems for such an implementation, as well as subsequent theoretical studies in the area of incident wave profile optimization, should investigate this effect.

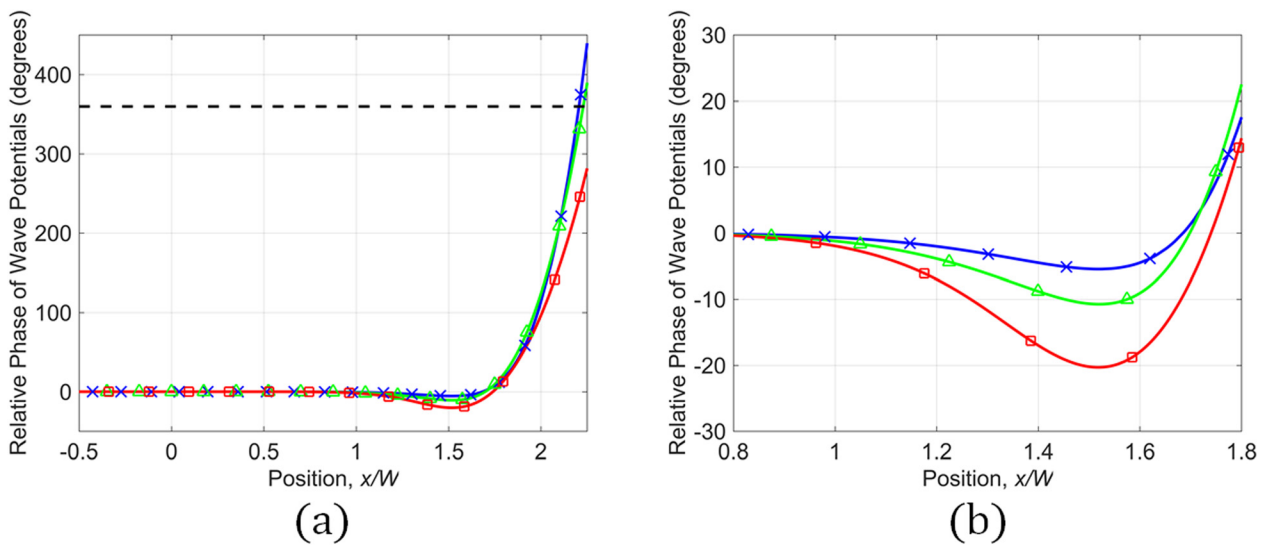

FIG. 10. (Color online) The relative phase distortion of an incident bounded wave profile at the interface ($z=0$) due to the propagation effect with the offset distance set at $h=25$ mm ($\times$ markers), $h=50$ mm (triangular markers), and $h=100$ mm (square markers). The incident wave has a half beamwidth of $W=20$ mm and a decay parameter of $\beta=200$ rad/m. The dashed line in (a) at 360° corresponds to no distortion, but leading one cycle relative to the 0° line. Note that (b) gives a zoomed-in view in the region near the amplitude peaks.

[1]F. R. Rollins, Jr., "Critical ultrasonic reflectivity: A neglected tool for material evaluation," Mater. Eval. **24**(12), 683–689 (1966).
[2]C. E. Fitch, Jr. and R. L. Richardson, "Ultrasonic wave models for nondestructive testing interfaces with attenuation," in *Progress in Applied Materials Research*, edited by E. G. Stanford, J. H. Fearon, and W. J. McGounagle (Iliffe Books, London, England, 1967), Vol. 8, pp. 79–120.
[3]K. Aki and P. G. Richards, *Quantitative Seismology: Theory and Methods* (W. H. Freeman and Company, San Francisco, CA, 1980), Vol. 1, 557 pp.
[4]J. Yang, N. DeRidder, C. Ume, and J. Jarzynski, "Non-contact optical fibre phased array generation of ultrasound for non-destructive evaluation of materials and processes," Ultrasonics **31**(6), 387–394 (1993).
[5]J. Peters, V. Kommareddy, Z. Liu, D. Fei, and D. Hsu, "Non-contact inspection of composites using air-coupled ultrasound," AIP Conf. Proc. **657**(22), 973–980 (2003).
[6]R. E. Green, "Non-contact ultrasonic techniques," Ultrasonics **42**(1), 9–16 (2004).
[7]L. Gao, K. J. Parker, R. M. Lerner, and S. F. Levinson, "Imaging of the elastic properties of tissue: A review," Ultrasound Med. Biol. **22**(8), 959–977 (1996).
[8]G. Rousseau, B. Gauthier, A. Blouin, and J. P. Monchalin, "Non-contact biomedical photoacoustic and ultrasound imaging," J. Biomed. Opt. **17**(6), 061217 (2012).
[9]M. C. Bhardwaj, "Innovation in non-contact ultrasonic analysis: Applications for hidden objects detection," Mater. Res. Innov. **1**(3), 188–196 (1997).
[10]T. H. Gan, P. Pallav, and D. A. Hutchins, "Non-contact ultrasonic quality measurements of food products," J. Food Eng. **77**(2), 239–247 (2006).
[11]S. Meyer, S. A. Hindle, J. P. Sandoz, T. H. Gan, and D. A. Hutchins, "Non-contact evaluation of milk-based products using air-coupled ultrasound," Measurement Sci. Technol. **17**(7), 1838–1846 (2006).
[12]L. M. Brekhovskikh, *Waves in Layered Media* (Academic Press, New York, 1960), 561 p.
[13]N. F. Declercq, R. Briers, J. Degrieck, and O. Leroy, "The history and properties of ultrasonic inhomogeneous waves," IEEE Trans. Ultrason. Ferroelectr. Frequency Control **52**(5), 776–791 (2005).
[14]J. D. N. Cheeke, *Fundamentals and Applications of Ultrasonic Waves* (CRC Press, Boca Raton, FL, 2012), pp. 125–134.
[15]H. L. Bertoni and T. Tamir, "Unified theory of Rayleigh-angle phenomena for acoustic beams at liquid-solid interfaces," Appl. Phys. **2**(4), 157–172 (1973).
[16]M. A. Breazeale, L. Adler, and L. Flax, "Reflection of a Gaussian ultrasonic beam from a liquid–solid interface," J. Acoust. Soc. Am. **56**(3), 866–872 (1974).
[17]M. A. Breazeale, L. Adler, and G. W. Scott, "Interaction of ultrasonic waves incident at the Rayleigh angle onto a liquid–solid interface," J. Appl. Phys. **48**(2), 530–537 (1977).
[18]T. D. Ngoc and W. G. Mayer, "Numerical integration method for reflected beam profiles near Rayleigh angle," J. Acoust. Soc. Am. **67**(4), 1149–1152 (1980).
[19]Y. Bouzidi and D. R. Schmitt, "Acoustic reflectivity goniometry of bounded ultrasonic pulses: Experimental verification of numerical models," J. Appl. Phys. **104**(6), 064914 (2008).
[20]N. F. Declercq and E. Lamkanfi, "Study by means of liquid side acoustic barrier of the influence of leaky Rayleigh waves on bounded beam reflection," Appl. Phys. Lett. **93**(5), 054103 (2008).
[21]N. F. Declercq, "Experimental study of ultrasonic beam sectors for energy conversion into Lamb waves and Rayleigh waves," Ultrasonics **54**(2), 609–613 (2014).
[22]S. Vanaverbeke, F. Windels, and O. Leroy, "The reflection of bounded inhomogeneous waves on a liquid/solid interface," J. Acoust. Soc. Am. **113**(1), 73–83 (2003).
[23]D. C. Woods, J. S. Bolton, and J. F. Rhoads, "On the use of evanescent plane waves for low-frequency energy transmission across material interfaces," J. Acoust. Soc. Am. **138**(4), 2062–2078 (2015).
[24]D. C. Woods, J. S. Bolton, and J. F. Rhoads, "Enhanced acoustic transmission into dissipative solid materials through the use of inhomogeneous plane waves," J. Phys. Conf. Ser. **744**(1), 012188 (2016).
[25]K. Van Den Abeele and O. Leroy, "On the influence of frequency and width of an ultrasonic bounded beam in the investigation of materials: Study in terms of heterogeneous plane waves," J. Acoust. Soc. Am. **93**(5), 2688–2699 (1993).
[26]N. F. Declercq and O. Leroy, "A feasibility study of the use of bounded beams resembling the shape of evanescent and inhomogeneous waves," Ultrasonics **51**(6), 752–757 (2011).
[27]H. Cox, R. Zeskind, and M. Owen, "Robust adaptive beamforming," IEEE Trans. Acoust. Speech Signal Processing **35**(10), 1365–1376 (1987).
[28]B. D. Van Veen and K. M. Buckley, "Beamforming: A versatile approach to spatial filtering," IEEE ASSP Mag. **5**(2), 4–24 (1988).
[29]J. Ahrens, M. R. Thomas, and I. Tashev, "Efficient implementation of the spectral division method for arbitrary virtual sound fields," in *Proceedings of the IEEE Workshop on Applications of Signal Processing to Audio and Acoustics*, New Paltz, NY (2013), pp. 1–4.
[30]O. Leroy, G. Quentin, and J. Claeys, "Energy conservation for inhomogeneous plane waves," J. Acoust. Soc. Am. **84**(1), 374–378 (1988).
[31]M. Deschamps, "Reflection and refraction of the evanescent plane wave on plane interfaces," J. Acoust. Soc. Am. **96**(5), 2841–2848 (1994).
[32]T. Tamir and H. L. Bertoni, "Lateral displacement of optical beams at multilayered and periodic structures," J. Opt. Soc. Am. **61**(10), 1397–1413 (1971).
[33]F. J. Lockett, "The reflection and refraction of waves at an interface between viscoelastic materials," J. Mech. Phys. Solids **10**(1), 53–64 (1962).
[34]H. F. Cooper, Jr. and E. L. Reiss, "Reflection of plane viscoelastic waves from plane boundaries," J. Acoust. Soc. Am. **39**(6), 1133–1138 (1966).
[35]R. D. Borcherdt, "Reflection–refraction of general P-and type-I S-waves in elastic and anelastic solids," Geophys. J. Int. **70**(3), 621–638 (1982).
[36]R. D. Borcherdt, *Viscoelastic Waves in Layered Media* (Cambridge University Press, Cambridge, UK, 2009), 328 pp.
[37]D. Trivett, L. Luker, S. Petrie, A. Van Buren, and J. Blue, "A planar array for the generation of evanescent waves," J. Acoust. Soc. Am. **87**(6), 2535–2540 (1990).
[38]O. Kirkeby and P. A. Nelson, "Reproduction of plane wave sound fields," J. Acoust. Soc. Am. **94**(5), 2992–3000 (1993).
[39]H. Itou, K. Furuya, and Y. Haneda, "Evanescent wave reproduction using linear array of loudspeakers," in *Proceedings of the IEEE Workshop on Applications of Signal Processing to Audio and Acoustics*, New Paltz, NY (2011), pp. 37–40.
[40]T. J. Matula and P. L. Marston, "Electromagnetic acoustic wave transducer for the generation of acoustic evanescent waves on membranes and optical and capacitor wave-number selective detectors," J. Acoust. Soc. Am. **93**(4), 2221–2227 (1993).